Available online at www.sciencedirect.com

SciVerse ScienceDirect

Ceramics International 38 (2012) 3445–3451

CERAMICS INTERNATIONAL

www.elsevier.com/locate/ceramint

An investigation on mechanical behavior of barium titanate foam with hydroxyapatite coating

Hoda Zarkoob [a,*], Saeed Ziaei-Rad [a], Mohammadhossein Fathi [b], Hossein Dadkhah [a]

[a] Department of Mechanical Engineering, Isfahan University of Technology, Isfahan 84156-83111, Iran

[b] Biomaterials Research Group, Department of Materials Engineering, Isfahan University of Technology, Isfahan 84156-83111, Iran

Received 13 August 2011; accepted 21 December 2011

Available online 12 January 2012

Abstract

In this study the mechanical behavior of barium titanate foam with hydroxyapatite coating under compressive loads was studied. The effect of foam's porosity and hydroxyapatite coating was investigated in uniaxial compression tests. The results show that the coating magnifies the pressure strength of the structure about five times and enhances its mechanical properties. The uniaxial compression test was simulated in a finite element package in which the porous structure was modeled by crushable foam material model. The results of simulation demonstrate a reasonable correspondence with the experimental data. The results also show that crushable foam material is a good candidate for modeling mechanical behavior of barium titanate foams under compression.

Keywords: Mechanical properties; Barium titanate foam; Hydroxyapatite coating; Finite element modeling

1. Introduction

Making composite is a suitable way to combine various properties of different materials and prepare a new material with desired characteristics [1]. Ceramic foams are a familiar group of composites that have been used in different industries for many years [2]. Corrosive filtration systems, thermal insulation, acoustic receiving systems, scaffolds and solid oxide fuel cells are different applications of ceramic foams in recent years [3]. For each application especial mechanical, electrical and chemical properties are required. In porous ceramics, the grain size, shape, wall thickness and cell window size of the voids has a principle effect on the mechanical and electrical properties of ceramic foams [4]; therefore, it is essential to investigate the effects of porosity and foaming process on different ceramic properties.

One of the most applicable electro active ceramics is barium titanate ($BaTiO_3$). High dielectric constant, piezoelectric and ferroelectric properties of this ceramic makes it proper for a large number of electrical applications [5]. In addition, biocompatible behavior of this ceramic [6] makes it a new candidate for being a bone graft material. Especially in porous form, barium titanate (BT) can be used as a scaffold for superseding bone tissue and also mimicking piezoelectric properties of bones [7].

Lately, it was reported that $BaTiO_3$ foam can be prepared with the direct foaming method using a liquid, two component polyurethane (PU) systems [4]. The fabrication of the PU system was based on the reaction between a disocyanate and a polyol that occurs in the presence of a catalyst. Wucherer et al. used a laboratory-developed and a commercial PU system to produce BT foams and evaluate their physical and mechanical properties [4,8]. In a separate study, the authors have synthesized porous BT with nanostructured hydroxyapatite (HA) coating and showed that the HA coating improve the bioactivity of porous samples. Preparing porous BT was carried out in a direct foaming method with polymeric polyurethane foam. Hydroxyapatite was then coated on the surface of the porous samples with the combination of sol–gel and dip-coating method [7]. The purpose of this study is investigating the mechanical behavior of porous barium titanate with hydroxyapatite coating and exploring the effect of porosity along with HA coating on BT's mechanical behavior.

In engineering applications, foams are regularly under compression; accordingly, for studying the mechanical

* Corresponding author. Tel.: +98 311 391 5244; fax: +98 311 391 2628.
E-mail address: hd.zarkoob@gmail.com (H. Zarkoob).

0272-8842/$36.00
doi:10.1016/j.ceramint.2011.12.057

behavior of the prepared porous samples, uniaxial compression test was carried out on prepared samples. In order to investigate the effect of porosity and also HA coating on mechanical properties of porous samples, four groups of compact and porous samples, with and without hydroxyapatite coating were tested. The compressive stress–strain diagram of the samples was depicted and comparisons between the results were obtained from compact/porous and coated/non-coated samples. Also, the porous structure was modeled in an in-house finite element package with crushable foam material. The results gained from simulations were compared with the experimental data to see if the crushable foam material model is a good choice for simulating mechanical behavior of BT foams. Finally, some discussions were provided on the obtained results.

2. Fabrication procedure

In this section the process of fabricating the porous barium titanate with HA coating will be explained briefly. Porous samples were prepared with commercial spray of polyurethane foam. Barium titanate powder (Merck, Germany) was mixed with PU foam (Bautechnik, Ceresite CS 360, Henkel, Germany) in volumetric ratio of 1/3. They were left away for 48 h to dry out. In sintering process, the samples were heated to 600 °C at 60 °C/min and hold in that temperature for 1 h to burn out polyurethanes completely. Afterwards, they were heated to 1150 °C at 150 °C/min and hold for 8 h to complete the sintering process [7]. The prepared samples were cut into cylindrical shapes with 12 mm diameter and 3 mm thickness.

Hydroxyapatite was coated on porous samples with the combination of sol–gel and deep coating method. In order to prepare HA sol at first 0.01 mL P_2O_5 and 0.0333 mL $Ca(NO_3)_2{\cdot}4H_2O$ was solved in 20 mL ethanol separately. When the dissolution processes were completed, they were mixed together and stirred for 1 h. Before changing the sol of the hydroxyapatite into gel, the samples were soaked in the solution and kept there for 3 h to saturate the whole voids of the porous samples. After aging for 24 h, the samples were dried out at 80 °C for 24 h and subsequently heated up to 600 °C at 5 °C/min and kept for 1 h [7]. The image of the prepared porous samples is shown in Fig. 1.

Fig. 1. The image of porous $BaTiO_3$ with HA coating.

Fig. 2. The image of compact $BaTiO_3$.

A group of compact samples were prepared to compare their mechanical behavior with the porous ones. Compact samples were produced using a cylindrical die with 150 MPa pressure. Poly vinyl alcohol (PVA) was used as a binder. During the sintering process the samples were held at 600 °C for 1 h until PVA burn out completely. Then, they were heated to 1100 °C and kept at this temperature for 8 h. The prepared samples had cylindrical shape with 12 mm diameter and 3 mm thickness. The image of the prepared compact samples is shown in Fig. 2.

3. Characterization

The porosity and density of the porous BT samples were determined by using Archemedes's method with distilled water as an immersion medium and the theoretical density of 6.02 g cm^{-3} for barium titanate [9]. The percentage of porosity in the prepared BT foam was $\%78 \pm 3$ and its density was 1.29 ± 0.04 g cm^{-3}. The results are the mean values of five measurements.

Also, the morphology of the porosities and the coating was investigated by using SEM (Philips XL30). SEM micrograph of non-coated samples (Fig. 3) shows the morphology and size of the foam voids. The micrographs show that the voids are spherical and that their diameters are between 50 μm and 500 μm.

Also, Fig. 4 shows the SEM image of the coated samples. The micrographs show that HA was coated on the voids' surfaces completely [7].

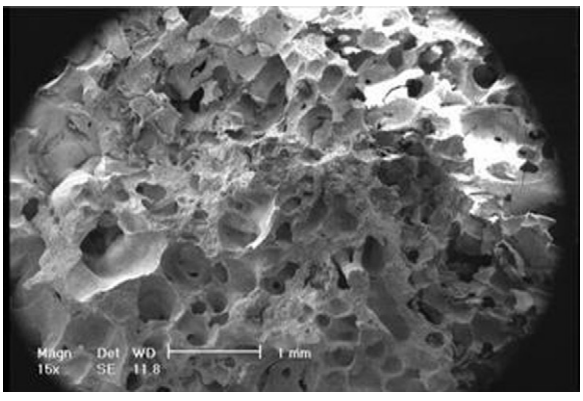

Fig. 3. SEM image of the non-coated samples.

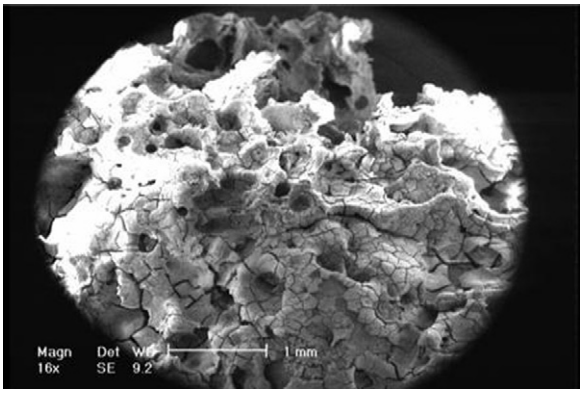

Fig. 4. SEM image of the coated samples.

4. Mechanical tests

In order to investigate the effect of porosity and HA coating on mechanical properties of BT foams, uniaxial compression test was carried out on compact and porous samples with and without HA coating. The test was done with a material test device (Zwick/Materialprufung1446). The device has two movable steel plates (Fig. 5). The relative displacement of these plates is controllable with a computer program. One of the plates has a force sensor and would measure the applied forces. In this study, each sample was put between these plates and the computer software programed to make a relative velocity of $v = 1.27$ mm/min between the plates. The force–displacement diagram of the samples was plotted with the measured force and the applied displacement.

Fig. 5. The uniaxial compression test machine with its two steel plates.

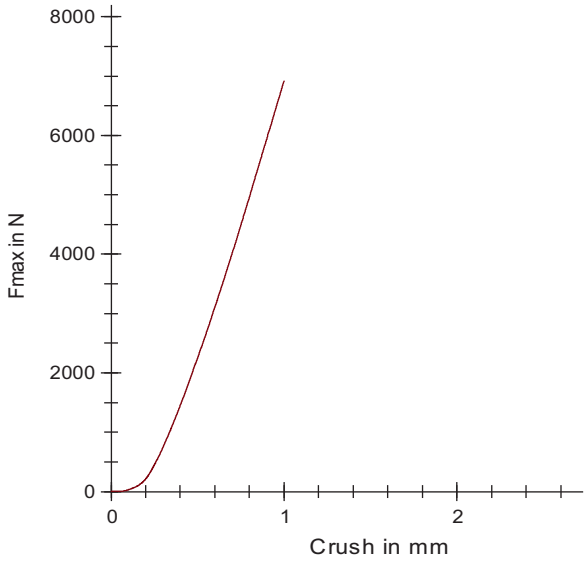

Fig. 6. Experimental force–displacement diagram of the compact BT disks without HA coating.

5. Experimental test results

Figs. 6–9 show the force–displacement diagram of the compact, porous coated and non-coated samples.

The local drop observed in the force–displacement diagrams of porous samples happens when large voids in the foam structure collapse. These local fails do not result in the failure of the whole structure; therefore they do not change the overall behavior of the force–displacement diagram. The compressive stress–strain of the samples was plotted under the $\nu = 0$ assumption for the ceramic samples. Figs. 10 and 11 show the compressive stress–strain obtained from the uniaxial compression test.

As Fig. 10 shows, the compressive stress–strain diagrams of compact BT disks were linear and the slop of the diagram in coated samples (213.12 MPa) is near the slop of the diagram in non-coated samples (207.414 MPa). It means that coating had not significant effect on the strength of compact BT disks.

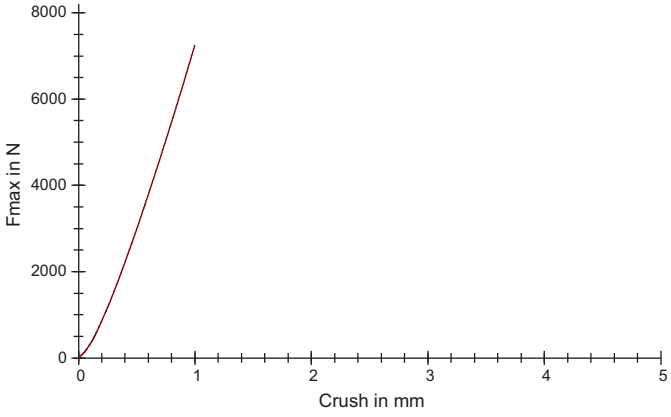

Fig. 7. Experimental force–displacement diagram of the compact BT disks with HA coating.

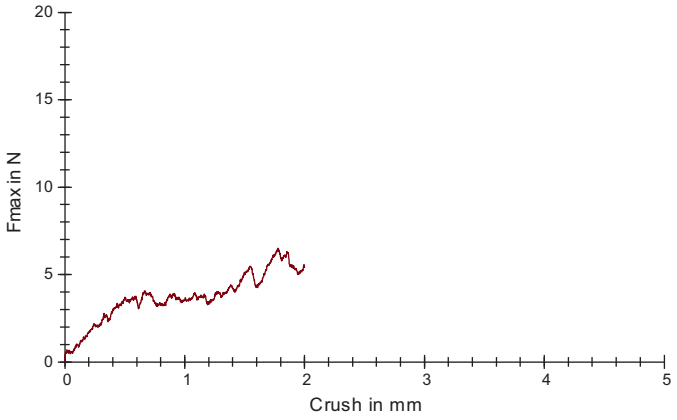

Fig. 8. Experimental force–displacement diagram of the porous BT disks without HA coating.

In compressive stress–strain diagrams of BT foams three definite regions was observed: linear elasticity, plateau and densification (Fig. 11). At small strains, usually less than 5%, the behavior is linear elastic. As the load increases, the foam cells begin to collapse by elastic buckling, plastic yielding or brittle crushing, depending on mechanical properties of the cell walls. Collapse progresses at roughly constant load, giving a stress plateau, until the opposing walls in the cells meet and touch, when densification causes the stress to increase steeply.

As Fig. 11 shows, the slop of the linear elastic part of diagram in coated samples is 0.754 MPa while the slop of the diagram in non-coated samples is 0.1662 MPa. It shows that the coating magnifies the pressure strength of the structure about five times and thus enhances the mechanical properties of the material significantly.

6. Theory

Crushable foam is a class of foam materials, which undergo permanent (plastic) deformation. The crushable foam plasticity models are used to model the enhanced ability of a foam material to deform in compression due to cell wall buckling processes [10–12]. The behavior of crushable foam material model under compressive loads has two parts: The elastic part

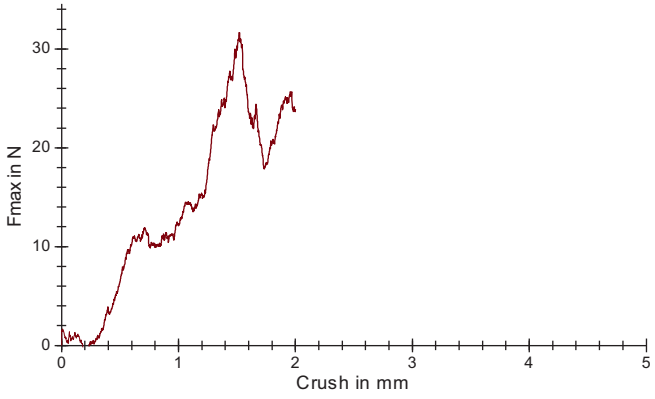

Fig. 9. Experimental force–displacement diagram of the porous BT disks with HA coating.

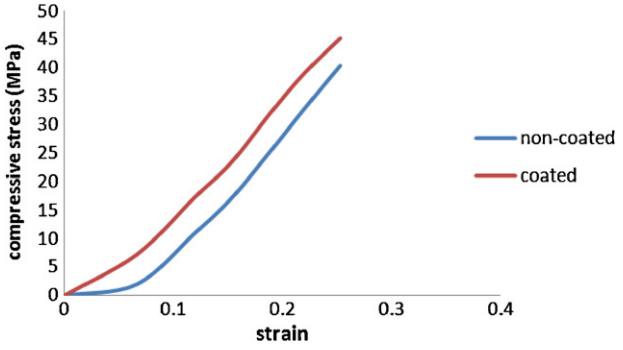

Fig. 10. Experimental compressive stress–strain diagrams of compact BT disks (coated and non-coated samples).

of the response which is specified as linear elastic behavior and the plastic part, which is defined with a hardening law. The hardening law determines the yield stress in uniaxial compression as a function of the value of the logarithmic plastic strain.

Two hardening models are available: the volumetric hardening model, the isotropic hardening model. The volumetric hardening was used in the modeling, and thus this will be explained briefly here.

6.1. Elastic behavior

The elastic behavior is modeled as linear elastic

$$\sigma = 2G(\varepsilon_d - \varepsilon_{dp}) - K(\varepsilon_\upsilon - \varepsilon_{\upsilon p})I \tag{1}$$

where ε_d, ε_{dp}, ε_υ and $\varepsilon_{\upsilon p}$ are deviatoric strain tensors, plastic deviatoric strain tensor, volumetric strain and plastic volumetric strain and σ, G, K are the second-order stress tensor, shear modulus and bulk modulus.

6.2. Plastic behavior

The yield surface and the flow potential for the crushable foam models are defined as:

$$f = \sqrt{q^2 + \alpha^2(p - p_0)^2} - B = 0 \tag{2}$$

$$g = \sqrt{q^2 + \beta^2 p^2} \tag{3}$$

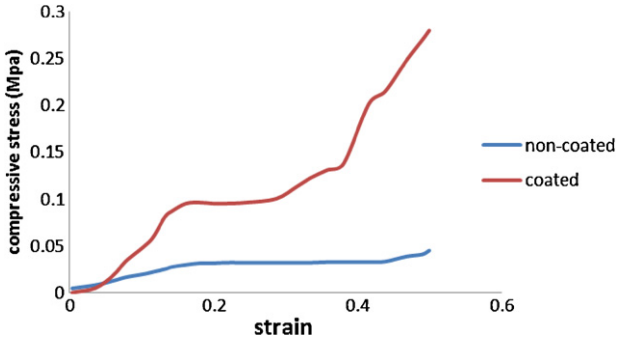

Fig. 11. Experimental compressive stress–strain diagrams of BT foam (coated and non-coated samples).

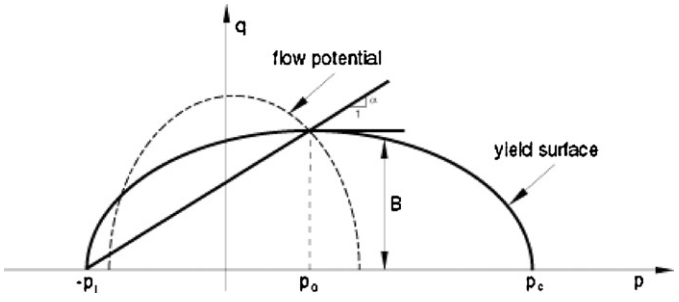

Fig. 12. Typical yield surface and flow potential for the crushable foam model.

where p, q are the pressure and Mises stresses. Parameters f and g can each be represented as an ellipse in the p–q stress plane with α and β representing the shape of the yield ellipse and the ellipse for the flow potential, respectively; p_0 is the center of the yield ellipse, and B is the length of the (vertical) q-axis of the yield ellipse. The flow potential is an ellipse centered in the origin. The yield surface and the flow potential are depicted in Fig. 12.

The parameters p_0 and B of the yield ellipse are related to the yield strength in hydrostatic compression, p_c, and to the yield strength in hydrostatic tension, p_t, by

$$p_0 = \frac{p_c - p_t}{2} \tag{4}$$

$$B = \alpha A = \alpha \frac{p_c + p_t}{2} \tag{5}$$

where p_c and p_t are positive quantities and A is the length of the (horizontal) p-axis of the yield ellipse. The shape factor, α, remains as a constant during any plastic deformation process. The evolution of the yield ellipse is controlled by a plastic strain measure, $\bar{\varepsilon}$, which is the volumetric compacting plastic strain, $-\varepsilon_{vol}^{pl}$, for the volumetric hardening model, and the equivalent plastic strain, $\bar{\varepsilon}^{pl}$ (to be defined later), for the isotropic hardening model. To define the hardening behavior, uniaxial compression test data are required. A piecewise linear hardening curve of uniaxial Cauchy stress versus axial (logarithmic) plastic strain must be entered in a tabular form.

6.3. Crushable foam model with volumetric hardening

The volumetric hardening model, assumes that the hydrostatic tension strength, p_t, remains constant throughout any plastic deformation process. By contrast, the hydrostatic compression strength evolves as a result of compaction (increase in density) or dilation (reduction in density) of the material:

$$p_c = p_c(\bar{\varepsilon}) \tag{6}$$

where

$$\bar{\varepsilon} \equiv -\varepsilon_{vol}^{pl} = -trace\,\varepsilon^{pl} \tag{7}$$

parameter α can be calculated from the initial yield strength in uniaxial compression, σ_c^0, taken as a positive value; the initial yield strength in hydrostatic compression, p_c^0; and the yield strength in hydrostatic tension, p_t; as

$$\alpha = \frac{3k}{\sqrt{(3k_t + k)(3 - k)}} \tag{8}$$

With

$$k = \frac{\sigma_c^0}{p_c^0}, k_t = \frac{p_t}{p_c^0} \tag{9}$$

where the yield stress ratios, k and k_t are provided by the user. For a valid yield surface the choice of yield stress ratios must be such that $0 < k < 3$ and $k_t \geq 0$. The yield surface is the Mises circle in the deviatoric stress plane.

The plastic strain rate for the volumetric hardening model is assumed to be

$$\dot{\varepsilon}^{pl} = \dot{\bar{\varepsilon}}^{pl} \frac{\partial g}{\partial \sigma} \tag{10}$$

where $\dot{\bar{\varepsilon}}^{pl}$ is the equivalent plastic strain rate defined as

$$\dot{\bar{\varepsilon}}^{pl} = \frac{\sigma : \dot{\varepsilon}^{pl}}{g} \tag{11}$$

and g is the flow potential, chosen in this model as

$$g = \sqrt{q^2 + \frac{9}{2} p^2} \tag{12}$$

This potential is a particular case of Eq. (3) with $\beta^2 = 9/2$. A geometrical representation of the flow potential in the p–q stress plane is shown in Fig. 13.

Eq. (12) gives a direction of flow that is identical to the stress direction for radial paths. It can be seen that the plastic flow is nonassociative. Therefore, the use of this foam model generally requires the solution of nonsymmetric equations.

The yield surface intersects the p-axis at $-p_t$ and p_c. We assume that p_t remains fixed throughout any plastic deformation process. By contrast, the compressive strength, p_c, evolves as a result of compaction (increase in density) or dilation (reduction in density) of the material. The evolution of the yield surface can be expressed through the evolution of the yield surface size on the hydrostatic stress axis, $p_t + p_c$, as a function of the value of volumetric compacting plastic strain, $-\varepsilon_{vol}^{pl}$. With p_t constant, this relation can be obtained from a user-provided uniaxial compression test data using

$$p_c(\varepsilon_{vol}^{pl}) = \frac{\sigma_c(\varepsilon_{axial}^{pl})[\sigma_c(\varepsilon_{axial}^{pl})(1/\alpha^2 + 1/9) + (p_t/3)]}{p_t + ((\sigma_c(\varepsilon_{axial}^{pl}/3))/3)} \tag{13}$$

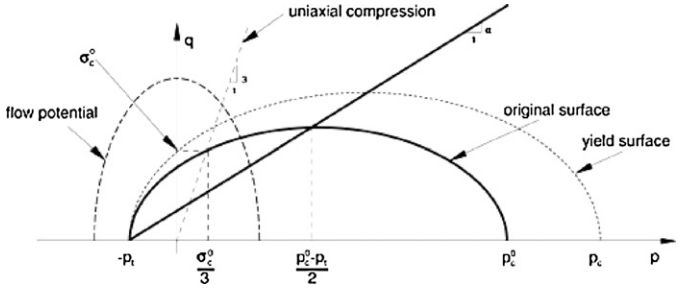

Fig. 13. Yield surfaces and flow potential for the volumetric hardening model.

along with the fact that $\varepsilon_{axial}^{pl} = \varepsilon_{vol}^{pl}$ in uniaxial compression (due to zero plastic Poisson's ratio). Thus, the user provides input to the hardening law by only specifying, in the usual tabular form, the value of the yield stress in uniaxial compression as a function of the absolute value of the axial plastic strain. The table must start with a zero plastic strain (corresponding to the virgin state of the material), and the tabular entries must be given in ascending magnitude of ε_{axial}^{pl}. If desired, the yield stress can also be a function of temperature and other predefined field variables.

7. Finite element modeling

The porous structure was modeled by an in-house finite element package. Crushable foam material model was used to simulate the compressive behavior of the prepared samples.

Therefore, the crushable foam plasticity model with volumetric hardening was selected to simulate the compressive behavior of the BT porous samples. The input data for defining the crushable foam material model is tabulated in Table 1.

While it was difficult to perform hydrostatic tension and hydrostatic compression test, the ratio of initial yield stress in uniaxial compression to initial yield stress in hydrostatic compression and the ratio of yield stress in hydrostatic tension to initial yield stress in hydrostatic compression were first assumed and then verified with the results of the tests.

The crushable foam model also needs yield stress, σ_y, and uniaxial plastic strain, ε_{axial}^{pl}, to calculate the hardening. Uniaxial plastic strain can be obtained from nominal engineering strain as shown:

$$\varepsilon_{axial}^{pl} = Ln(1 + \varepsilon_{nom}) - \varepsilon^{pl} \tag{14}$$

where ε_{nom} is the nominal engineering strain (negative in compression) [11]. The yield stress and nominal engineering strain data were measured from single loading test.

The specimen's geometry was modeled with a 3D cylinder ($d = 12$ mm and $t = 3$ mm). The model was meshed using 8-node 3D solid elements. It was composed of 324 elements with 54 elements through the surface and 50 elements along the height of the specimen.

The compressive load of the uniaxial compression test was modeled in two different ways: (a) Type 1:Applying displacement boundary condition, $d = 0$ at the bottom plate and $v = 1.27$ mm/min (the rate of displacement in the real test) at the top plate (Fig. 14), (b) Type 2: Modeling two steel plates to apply the compression on the sample (Fig. 15). The steel plates were meshed using 4-node 2D shell elements. The top plate, moved with the rate of 1.27 mm/min toward the sample, was composed of 400 elements with 20 elements through the width and 20 elements along the length of the specimen. The bottom plate was composed of 100 elements with 10 elements through the width and 10 elements along the length of the specimen. The nodes on one side of the bottom plate were fixed with by applying displacement boundary conditions $d_x = 0$, $d_y = 0$ and $d_z = 0$. It should be noted that before carrying-out further computations, a mesh sensitivity study was performed with respect to the number of elements in order to ensure that the mesh was fine enough to give reliable results. The contact between the plates and the specimen were defined with surface-to-surface contacts.

Table 1
Characteristics of the fabricated BT foam.

Parameter	Value
Foam density	1.29 gr cm^{-3}
Elastic modulus of linear part	0.754 MPa
Poisson's ratio	0
The ratio of initial yield stress in uniaxial compression to initial yield stress in hydrostatic compression	1.1
The ratio of yield stress in hydrostatic tension to initial yield stress in hydrostatic compression	0.05

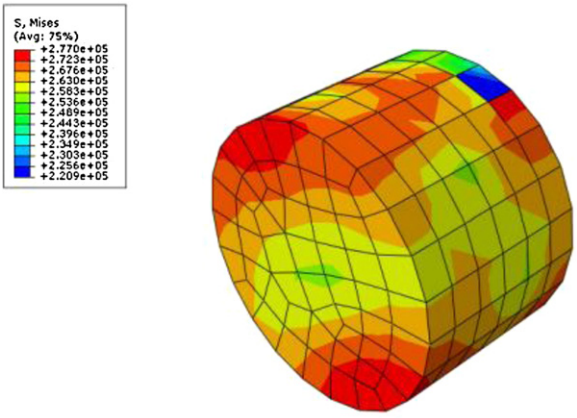

Fig. 14. Modeling the uniaxial compression test with type 1 boundary condition.

Moreover, as the problem was quasi-static, both implicit and explicit solver was used to perform the problem. Finally, the finite element results of two test modeling and two solution techniques were compared with experimental data of the uniaxial compression test.

8. Numerical results

Figs. 16 and 17 show the diagrams obtained from finite element with two types of boundary conditions together with the measured data.

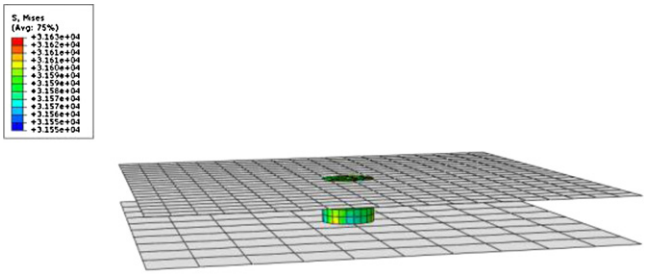

Fig. 15. Modeling the uniaxial compression test with type 2 boundary condition.

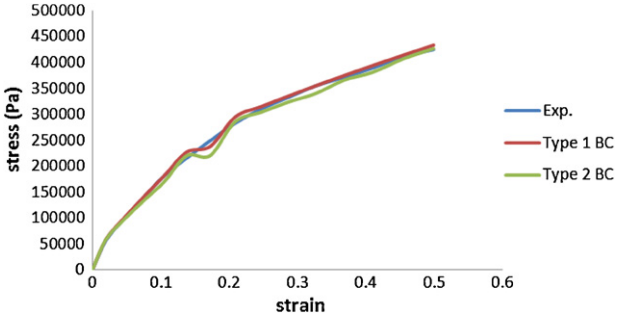

Fig. 16. Compressive stress–strain plots of porous BT (Experimental diagram, Type 1 and Type 2 BCs).

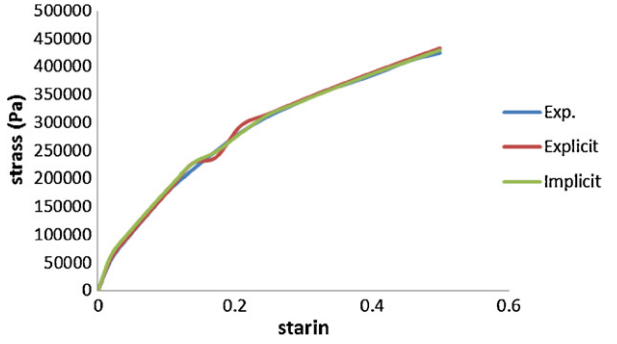

Fig. 17. Compressive stress–strain plots of porous BT (Experimental diagram, results from explicit and implicit solvers).

Fig. 16 shows that the results of modeling of the porous material with Type 1 B.C. have more correspondence with real test results. This is expected while defining contacts in modeling may cause some increase on the absolute errors. Also Fig. 17 demonstrates that solving the problem with the implicit solver has achieved better results in compare with the explicit solver. It is necessary to mention that due to the high degree of non-linearity in the problem, convergence of the results by implicit solving is not an easy task.

Overall, as the diagrams show, the theoretical results demonstrate a reasonable correspondence with the experimental data. It shows that crushable foam material model was a good option for modeling mechanical behavior of BT foams.

9. Conclusion

In this study the mechanical behavior of a foam composite made of porous Barium titanate with nano structured Hydroxyapatite coating under uniaxial compression was studied. The test results were then simulated by a developed finite element model.

The compressive stress–strain diagram of the samples that was obtained from uniaxial compression test results shows that the coating magnifies the pressure strength of the composite about five times and enhances its mechanical properties but it had no significant effect on strengthen of the compact disks.

Also, the porous structure was modeled by an in-house finite element package with crushable foam material model. The numerical results gained from the simulation shows good agreement with the measured data. The results show that crushable foam material model was a good option for modeling the mechanical behavior of fabricated BT foams under compression.

Acknowledgement

The authors are grateful to Isfahan University of Technology for supporting this research.

References

[1] F.L. Matthews, R.D. Rawlings, Composite Materials: Engineering and Science, CRC Press, Boca Raton, 1999.
[2] P. Colombo, M. Scheffler, Cellular Ceramics: Structure, Manufacturing and Applications, vol. 53, Wiley-VCH Verlag, Weinheim, Germany, 2000
[3] J.D. Green, P. Colombo, Cellular ceramic: intriguing structure, novel properties and innovative applications, MRS Bull. 28 (4) (2003) 296–300.
[4] L. Wucherer, J.C. Nino, F. Basoli, E. Traversa, Synthesis and characterization of $BaTiO_3$-based foams with a controlled microstructure, Int. J. Appl. Ceram. Technol. 6 (6) (2009) 651–660.
[5] A. Rae, M. Chu, V. Ganine, in: K.M. Nair, A.S. Bhalla (Eds.), $BaTiO_3$-Past, Present, and Future, in Dielectric Ceramic Materials, 1999, 1–12.
[6] F.R. Baxter, I.G. Turner, C.R. Bowen, J.P. Gittings, J.B. Chaudhuri, An in vitro study of electrically active hydroxyapatite-barium titanateceramics using Saos-2 cells, J. Mater. Sci. Mater. Med. 20 (2009) 1697–1708.
[7] H. Zarkoob, Synthesis, characterization and bioactivity evaluation of porous barium titanate with nanostructured hydroxyapatite coating for biomedical application, MSc Thesis, Mechanical Engineering Department, Isfahan University of Technology, 2011.
[8] L. Wucherer, J.C. Nino, G. Subhash, Mechanical properties of $BaTiO_3$ open-porosity foams, J. Eur. Ceram. Soc. 29 (2009) 1987–1993.
[9] R. Askeland, The Science and Engineering of Materials, 2nd ed., PWS Pub. Co., 1989.
[10] V.I. Rizov, Elastic–plastic response of structural foams subjected to localized static loads, Mater. Des. 27 (2006) 947–954.
[11] U.E. Ozturk, G. Anlas, Finite element analysis of expanded polystyrene foam under multiple compressive loading and unloading, Mater. Des. 32 (2011) 773–780.
[12] K.M. Ryu, J.Y. An, W.S. Cho, Y.C. Yoo, H.S. Kim, Mechanical modeling of Al–Mg alloy open-cell foams, Mater. Trans. 46 (3) (2005) 622–625.